Proc. 12th Int. Conf. Low Energy Antiproton Physics (LEAP2016)
JPS Conf. Proc. **18**, 011007 (2017)
https://doi.org/10.7566/JPSCP.18.011007

Progress of antihydrogen beam production using a double cusp trap

Y. Nagata[1,2], N. Kuroda[3], P. Dupre[2], B. Radics[2], M. Tajima[3,2], A. A. Capon[4], M. Diermaier[4], C. Kaga[5], B. Kolbinger[4], M. Leali[6], E. Lodi Rizzini[6], C. Malbrunot[7,4], V. Mascagna[6], O. Massiczek[4], T. Matsudate[3], C. Sauerzopf[4], M. C. Simon[4], K. Suzuki[4], J. Zmeskal[4], H. Breuker[7], H. Higaki[5], Y. Kanai[2], Y. Matsuda[3], S. Ulmer[8], L. Venturelli[6], E. Widmann[4], Y. Yamazaki[2],

[1]*Department of Applied Physics, Tokyo University of Agriculture and Technology, Koganei, Tokyo 184-8588, Japan*
[2]*Atomic physics research unit, RIKEN, Wako, Saitama 351-0198, Japan*
[3]*Graduate School of Arts and Sciences, The University of Tokyo, Komaba, Meguro, Tokyo 153-8902, Japan*
[4]*Stefan Meyer Institute for Subatomic Physics, Boltzmanngasse 3,1090 Vienna, Austria*
[5]*Graduate School of Advanced Sciences of Matter, Hiroshima University, Higashi-Hiroshima, Hiroshima 739-8530 Japan*
[6]*Dipartimento di Ingegneria dell'Informazione, Università di Brescia & Istituto Nazionale di Fisica Nucleare, Gruppo Collegato di Brescia, 25133 Brescia, Italy*
[7]*CERN, 1211 Geneva 23, Switzerland*
[8]*Ulmer Initiative Research Unit, RIKEN, Wako, Saitama 351-0198, Japan*

E-mail: ynagata@cc.tuat.ac.jp

(Received June 15, 2016)

We report the progress of the $\bar{H}$ beam production experiment and recent developments of the double cusp trap to improve of the beam intensity of the $\bar{H}$ atomic beams, the ASACUSA Micromegas tracker to monitoring the antihydrogen synthesis and the antihydrogen beam detector.

KEYWORDS: Antihydrogen, CPT invariance, Atomic beam

1. Introduction

CPT symmetry, corresponding to invariance under simultaneous charge (C), parity (P) and time (T) transformation, is believed to be one of the fundamental symmetries in nature. For example, all the relativistic quantum field theories of the Standard Model (SM) are CPT invariant. On the other hand, a plethora of phenomena which cannot be explained by SM were discovered. E.g. the unambiguous observation of neutrino oscillations implies non-zero neutrino mass, where the SM predicts the neutrino mass to be zero. This requires theories beyond the SM to explain these phenomena, some of them may violate CPT symmetry [1]. On the experimental side only a few precise tests of CPT invariance exist, which motivates and inspires further precise tests of CPT invariance, some of them are comparing the fundamental properties of matter and antimatter conjugates with high precision.

Several groups proposed precise experimental test of CPT invariance using antihydrogen ($\bar{H}$) atoms. Some target precision spectroscopy of the 1S-2S transition [2, 3] we, the ASACUSA collaboration, are focusing on hyperfine spectroscopy [1, 4].

In 2012 we succeeded in producing the first antihydrogen beams ever observed [5]. Since then, we are developing sensitive apparatuses to achieve our goal to perform hyperfine spectroscopy of $\bar{H}$ atoms with a fractional precision at the ppm level, at least.

According to the prominent Standard Model Extension (SME) which discusses effects of CPT and Lorentz violating fields to experimental systems [6,7], the violating factors shift the energy levels of $\bar{\mathrm{H}}$ atoms. It is important to note that as a consequence of the SME absolute precision is a more appropriate measure to characterize the sensitivity of an experiment with respect to CPT violation than the fractional precision. In this context the ground state hyperfine spectroscopy turns out to be a highly attractive probe for a search of CPT violating effects.

This paper summarizes our achievements, developments and upgrades of the experimental apparatus carried-out in recent years.

2. Hyperfine spectroscopy of the $\bar{\mathrm{H}}$ atom

The $\bar{\mathrm{H}}$ atom is electrically neutral, but has a magnetic moment $\boldsymbol{\mu}$. The interaction energy of the $\bar{\mathrm{H}}$ atom in a magnetic field $\boldsymbol{B}$ is $\phi = -\boldsymbol{\mu}\cdot\boldsymbol{B}$. The force acting on the $\bar{\mathrm{H}}$ atoms is written as $\boldsymbol{F} = -\boldsymbol{\nabla}\phi$. If $\boldsymbol{\mu}$ is a constant, $\boldsymbol{F} = \mu\boldsymbol{\nabla}|\boldsymbol{B}|$. To first order, the force is proportional to the gradient of the magnetic field strength. Therefore the $\bar{\mathrm{H}}$ atoms can be manipulated by magnetic field. The direction of the force is determined by the sign of μ. Figure 1 shows the magnetic field dependence of the energy levels of the ground state $\bar{\mathrm{H}}$ atoms. In the magnetic field, the energy levels of the $\bar{\mathrm{H}}$ atoms split into four. The energy levels of the upper two states increase as $\boldsymbol{B}$ increases. These states are attracted toward the lower field region, and hence are called as low field seeking (LFS) states. In contrast, the lower two states are attracted toward the higher field region, and hence are called as high field seeking (HFS) states.

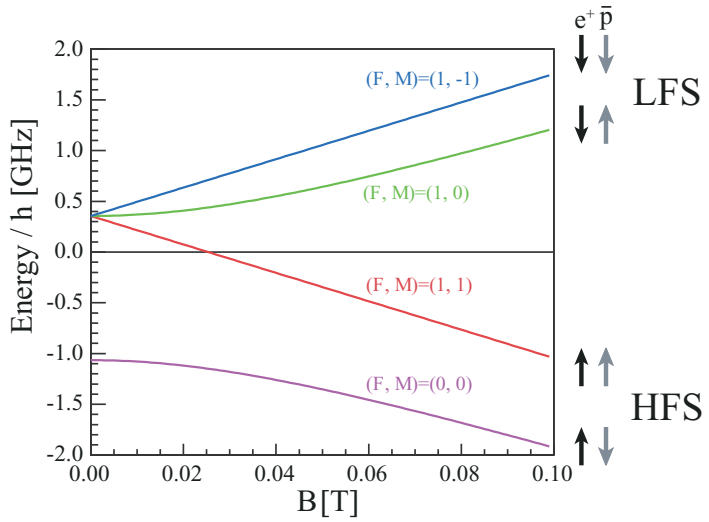

Fig. 1. The magnetic field dependence of the hyperfine energy levels of the ground-state $\bar{\mathrm{H}}$ atom in GHz. Upper two states are the low field seeking (LFS) states. Lower two states are the high field seeking (HFS) states.

Figure 2 (a) is a conceptual drawing to the measure the hyperfine transition frequency. The atomic beam is produced in the beam source and then polarized to LFS by the beam polarizer. The LFS beam passes through the microwave cavity and the LFS state analyzer which focuses the LFS beam on the beam detector. If the microwave frequency coincides with the hyperfine transition frequency, the atomic state turns from LFS to HFS. The HFS beam is diverged by the LFS state analyzer which leads to a decrease of signal on the beam detector. Therefore the hyperfine frequency is determined by measuring the counts of atoms as a function of the microwave frequency.

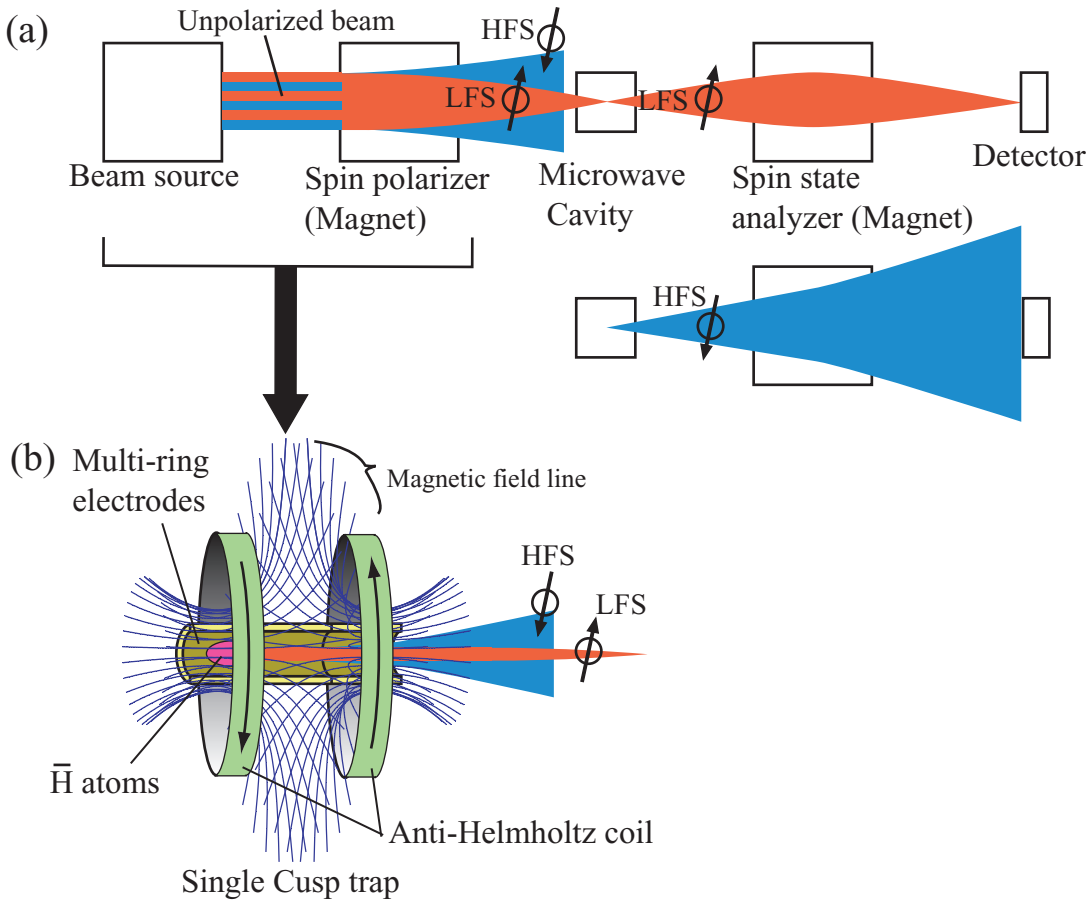

Fig. 2. (a) The conceptual figure for the measurement of the hyperfine frequency of the $\bar{\mathrm{H}}$ atom which consists of a beam source, the spin polarizer, a microwave cavity, a spin state analyzer, and a detector. (b) The conceptual figure of the single cusp trap.

In our experiment, we developed the single cusp trap (see Fig. 2 (b)) which has two functions, the $\bar{\mathrm{H}}$ atom synthesizer and the beam polarizer [11]. Thus this trap can improve the beam intensity in comparison with the two-step setup of the beam source and the polarizer in Fig. 2 (a). The single cusp trap consisted of the superconducting anti-Helmholtz coil (single cusp magnet) and the multi-ring electrodes for charged particle manipulation. The $\bar{\mathrm{H}}$ atoms were synthesized in this trap in 2010 [12]. The $\bar{\mathrm{H}}$ atomic beams were produced for the first time in 2012 [5].

2.1 Polarized $\bar{\mathrm{H}}$ beams from the single cusp magnet

As shown in Fig. 2 (b), the single cusp magnet consists of a two coil assembly having opposite current direction. Thus the magnetic field is zero at the center and increases with the distance from the center. The single cusp magnet produced a large magnetic field gradient. Figure 3 (a) shows the magnetic field strength $|\boldsymbol{B}|$ of the single cusp trap, where z and r show axial and radial coordinates, respectively. The arrow shows the direction of $\bar{\mathrm{H}}$ atom motion. The maximum magnetic field $|\boldsymbol{B}|$ on axis is 2.7 T at $z = \pm 0.14$ m from the center of the magnet.

In Fig. 3 (a), the magnetic field strength along r looks the harmonic in the radial direction. For example, at around the center of the magnet, the magnetic field strength is expressed as,

$$|\boldsymbol{B}| \propto \sqrt{r^2 + 4z^2}. \tag{1}$$

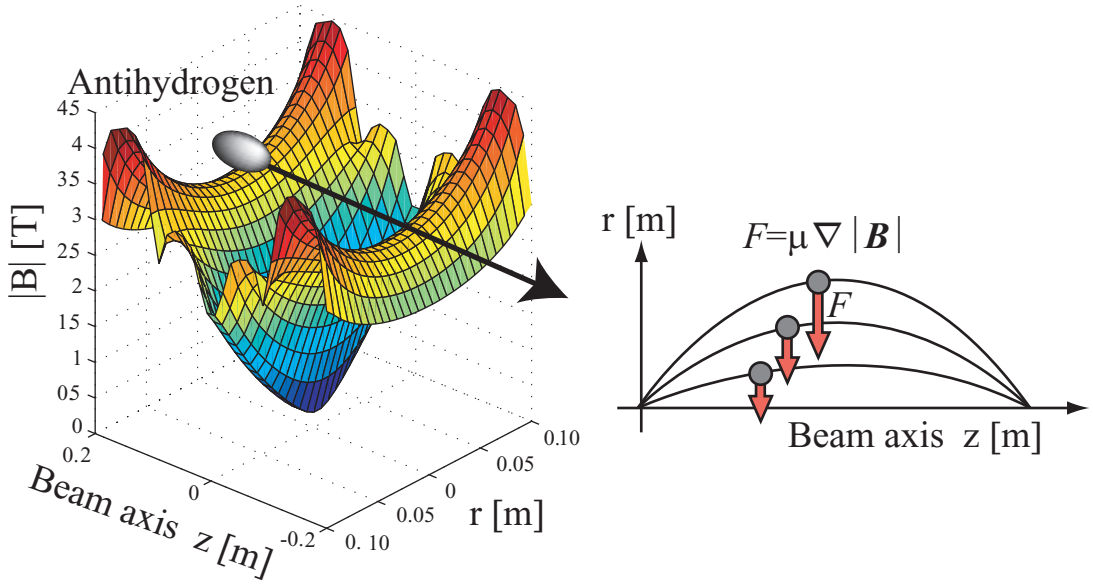

Fig. 3. (a) The magnetic field strength of the single cusp trap. The arrow shows the direction of the $\bar{\mathrm{H}}$ atom traveling to the downstream. (b) The schematic figure of the $\bar{\mathrm{H}}$ trajectories in the harmonic magnetic field. The axial velocities of the $\bar{\mathrm{H}}$ atoms are same.

For $z = 0$, $\partial|\boldsymbol{B}|/\partial r$ along r is constant. For $z > r$, $|\boldsymbol{B}| \propto \sqrt{r^2 + 4z^2} \sim 2z + \frac{r^2}{4z}$. Although $|\boldsymbol{B}|$ depends on the z position, we can treat the field as a simple harmonic field for $\bar{\mathrm{H}}$ atoms if the radial position of $\bar{\mathrm{H}}$ motion is not change very much. The details are discussed in [13]. The motions of the $\bar{\mathrm{H}}$ atoms are schematically shown in Fig. 3 (b) for the harmonic force. In this field, atoms with different velocities starting from the origin can return to the axis at the same time interval. If the velocities of the atoms along the beam axis are identical, the atoms return to the same position. Therefore the atoms can be focused by the single cusp magnet. The focusing performance and the polarization were calculated and reported in [13].

3. Experimental setup

Figure 4 shows a schematic view of the main part of our experimental setup. MUSASHI trap [15–17], a positron accumulator with a ^{22}Na source [18], and the double cusp trap are used for the $\bar{\mathrm{H}}$ synthesis and the production of $\bar{\mathrm{H}}$ beams. Antiprotons at 5.3 MeV are delivered by the antiproton decelerator of CERN. The particles are further decelerated down to 115 keV by a radio frequency quadrupole decelerator. Those antiprotons are injected into the MUSASHI trap. 10^6 antiprotons were caught and cooled down to sub-eV energies in the MUSASHI trap. The positron accumulator confined 1.5×10^7 positrons from the ^{22}Na source for 30 s.

For the spectroscopy line, a field ionizer, a microwave cavity, a sextupole magnet and an $\bar{\mathrm{H}}$ beam detector were developed as shown in Fig. 6. The field ionizer was developed for the ionizations of the $\bar{\mathrm{H}}$ atoms having the principal quantum number $n \gtrsim 12$ by applying the voltage differences up to 20 kV on the meshes. The microwave cavity for 1.42 GHz is used for the measurement of the hyperfine splitting. The sextupole magnet is the spin state analyzer for LFS and HFS $\bar{\mathrm{H}}$ atoms. Its magnetic field is harmonic in the radial direction, and increases with the distance from the axis, where the field on axis is zero. The LFS and HFS beams are focused and defocused on the $\bar{\mathrm{H}}$ beam detector by the magnet, respectively. The simulation code for the $\bar{\mathrm{H}}$ atoms traveling in the spectroscopy line was developed with the GEANT4 tool kit [24]. To study the precision of the spectroscopy, the reference

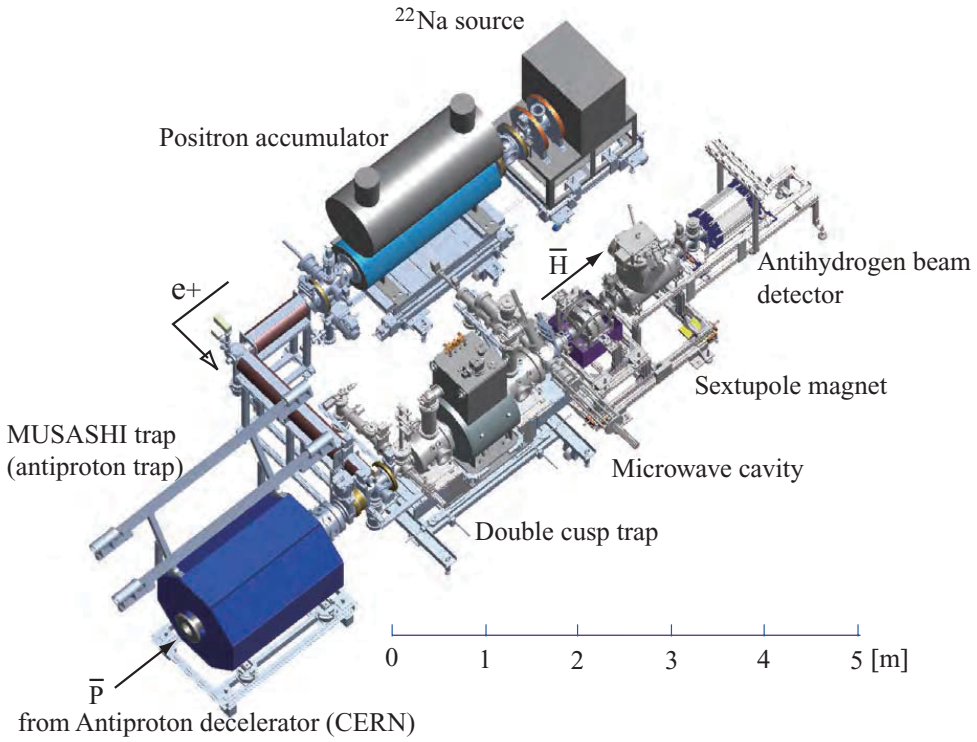

Fig. 4. The schematic drawing of the main part of the experimental setup for the production of the $\bar{H}$ atomic beams and the hyperfine spectroscopy. A MUSASHI trap, a positron accumulator with ^{22}Na and the double cusp trap are used for the $\bar{H}$ atom synthesizer and the $\bar{H}$ beam producer. A field ionizer, a microwave cavity, a sextupole magnet, and an $\bar{H}$ beam detector are used for the hyperfine spectroscopy line.

experiment was going on using atomic hydrogen beams [25].

In these apparatus, we describe the details of the double cusp trap, the AMT and $\bar{H}$ detector in the following subsections.

3.1 The double cusp trap

In 2014, we upgraded the single cusp magnet to a double cusp magnet to improve the $\bar{H}$ beam intensity and the polarization [14]. Figure 5 shows a schematic view of the double cusp trap. The double cusp trap has two sets of anti-Helmholtz coils (double cusp magnet) as well as the multi-ring electrodes similar to the single cusp assembly. In the double cusp magnet, the two central coils have the currents in the same directions. The currents on both sides are opposite directions to the center. These currents generate a main peak of 3.1 T at the center and sub peaks of −2.1 T and −1.9 T on axis. Therfore the double cusp magnet has two positions of $B = 0$ and high magnetic field gradients. This leads a high focusing performance. The $\bar{H}$ synthesis was performed in the upstream sub peak region (−2.1 T). The magnetic field strength $|\boldsymbol{B}|$ of the double cusp magnet is shown in Fig. 5 (b), where z and r show axial and radial coordinates, respectively. This field also looks harmonic toward r. The trajectory calculations were performed to evaluate the intensity of the $\bar{H}$ beams. The starting point is 0.26 m upstream from the center of the magnet. Initial emission directions are assumed to be isotropic. For example, for the $\bar{H}$ atoms with a kinetic energy of 10 K, the intensity of the LFS beam from the double cusp magnet is roughly 10 times larger than the single cusp magnet results in [13]. The details will be published.

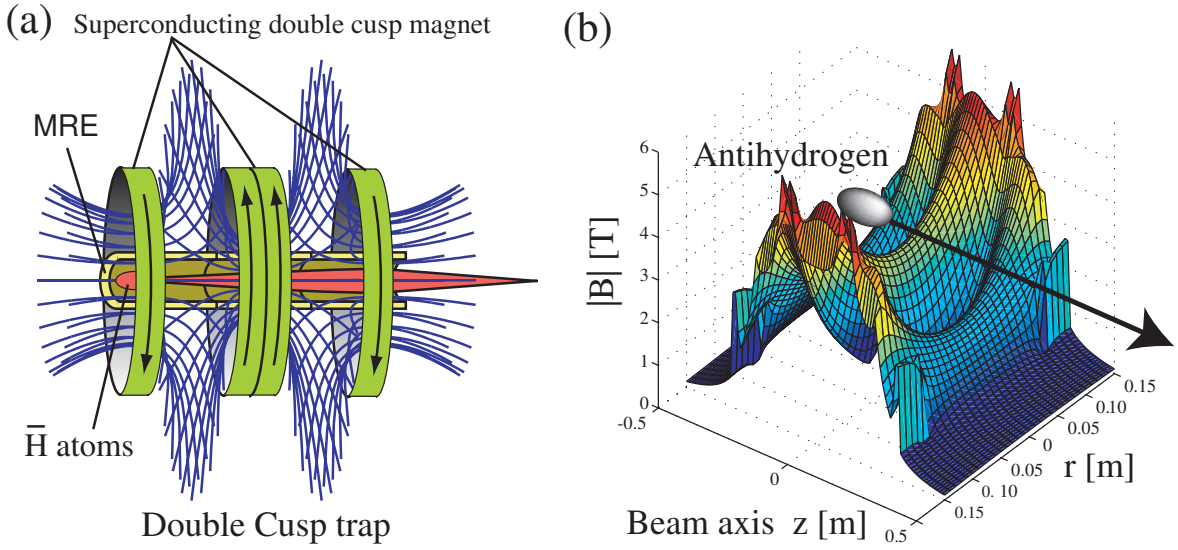

Fig. 5. (a) Schematic view of the double cusp trap which consists of two sets of Anti-Helmholtz coil (double cusp magnet) and the multi-ring electrodes. (b) The magnetic field strength of the double cusp magnet. The arrow shows the direction of the $\bar{H}$ atom traveling to the downstream.

3.2 The ASACUSA Micromegas tracker (AMT)

The ASACUSA Micromegas tracker (AMT) was developed for monitering the $\bar{H}$ annihilations in the double cusp trap as shown in Fig. 6 (a) [20, 21]. The AMT was installed between the double cusp magnet and the vacuum duct. The AMT has two half-cylinder layers of Micromegas with the active area of 400 mm for the axial direction. The radii of inner and outer layers are 78.5 mm and 88.5 mm, respectively. The AMT can reconstruct particle tracks. When $\bar{H}$ atoms annihilate, three charged pions are created in average. The each Micromegas measures the hit position of the pion as shown in Fig. 6 (b). The particle tracks are reconstructed with hit positions in two layers. The annihilation point of the antiproton or the $\bar{H}$ atom is determined from more than two particle tracks. The AMT monitors the annihilation signals during the mixing of antiprotons and positrons in the double cusp trap. In the AMT, 8 plastic scintillator bars are integrated to create the fast trigger for the readout of the Micromegas.

3.3 The $\bar{H}$ beam detector

The $\bar{H}$ beam detector was improved from the experiment in 2012 as shown in Fig. 7. The detector consisting of a position sensitive BGO ($Bi_4Ge_3O_{12}$) calorimeter [26] and a hodoscope were developed to count the number of the $\bar{H}$ atoms arriving at the detector. The BGO calorimeter measures the energy deposits of $\bar{H}$ atoms in the BGO and the positions where $\bar{H}$ atoms hit. The BGO scintillator whose diameter and thickness are 90 mm and 5 mm, respectively, are placed on a viewport glass in the UHV. The scintillation lights are detected by 4 multi-anode PMTs through the viewport glass. The uniformity is calibrated using the LED flashing on the MAPMT directly. The energy of the detector was calibrated with cosmic rays passing through the BGO crystal. The hodoscope has two layers of the 32 plastic scintillator bars. The hit positions of the charged particles were measured for each layer. The tracks of the charged particles were reconstructed with these positions and the position obtained by the BGO detector. The $\bar{H}$ atoms was expected to be identified by the analysis with the information of energy deposit and tracks against the cosmic ray background noises. The detector was tested with cosmic rays.

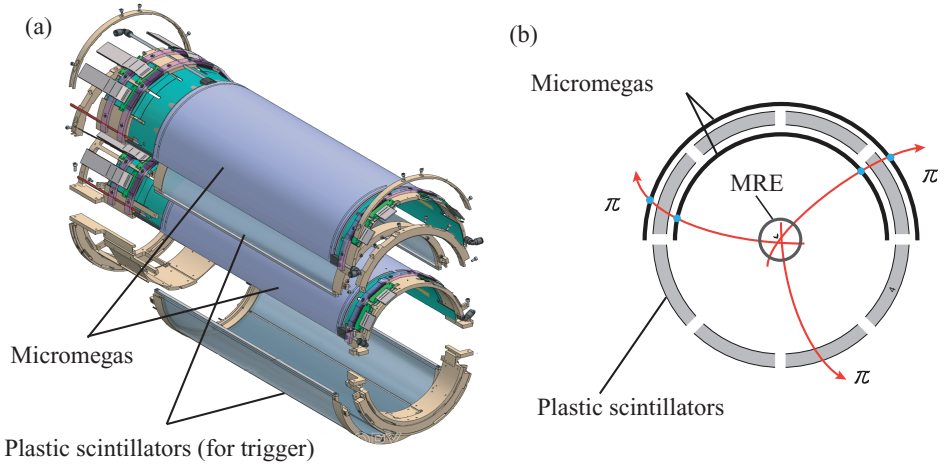

Fig. 6. (a) The ASACUSA Micromegas tracker (AMT). (b) The schenatic drawing of the cross section of the AMT.

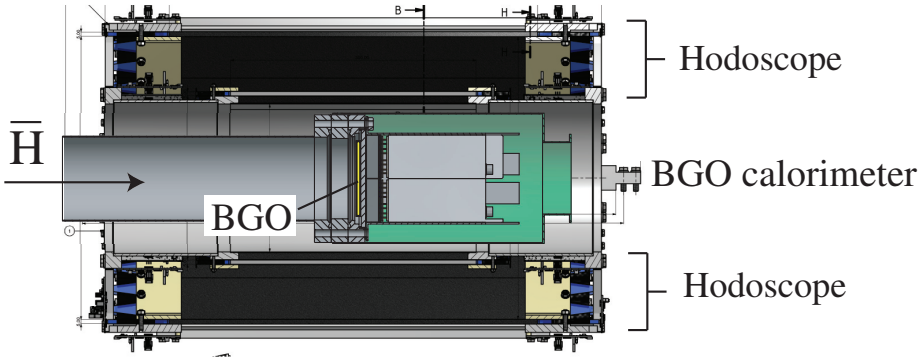

Fig. 7. The $\bar{H}$ beam detector consisting of the two-dimensional BGO calorimeter and the hodoscope.

4. Experiments

Figure 8 (a) shows the electric potential on axis in the MRE of the double cusp trap. The positrons are transported into the MRE of the double cusp trap. Typically $\times 10^8$ positrons are confined and compressed at the centre of the nested well. The potential is opened (green solid line) when about 3×10^5 antiprotons with low energy spread are injected from the MUSASHI trap into the positrons. A part of the $\bar{H}$ atoms in highly excited states passes a field ionization well , see Fig. 8 (a), and are ionized. The remaining antiprotons are confined in the field ionization well. After 20 s, these antiprotons are extracted by a fast pulse. Figure 8 (c) shows the example of the annihilation counts of these antiprotons measured by the AMT scintillators, where the antiproton injection energy was 150 eV. This indicates $\bar{H}$ atoms have been created [22]. To improve the $\bar{H}$ synthesis rate, we tried to change the antiproton injection in the energy lower than 150 eV [23].

Figure 9 shows the example of the reconstructed annihilation positions by the AMT for the first 3 second of the mixing after the injection of 20 eV antiprotons, respectively. Horizontal and vertical axes show axial and radial coordinates. Annihilations are observed at 4cm line which corresponds to the inner radius of the MRE. These were expected to be the $\bar{H}$ candidates because they were neutral and escaped from the nested well.

Figure 10 shows the example of the cosmic ray event. The BGO calorimeter shown by the center

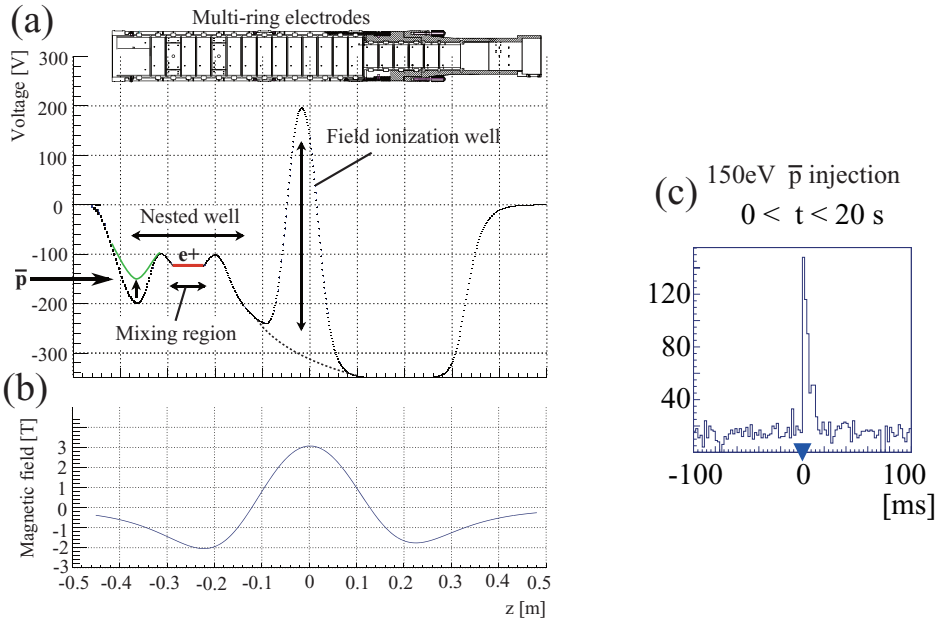

Fig. 8. (a) The electric potential on axis in the MRE. (b) The magnetic field on axis. (c) The annihilation counts of antiprotons measured by the AMT scintillators.

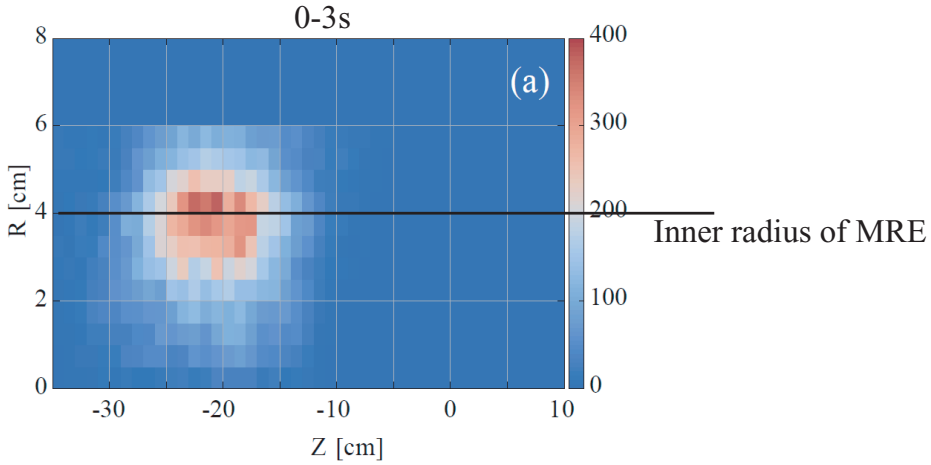

Fig. 9. The reconstructed annihilation positions by the AMT for first 3 second of the mixing after the injection of the antiprotons. Horizontal and vertical axes show axial and radial coordinates, respectively. Annihilations were observed at 4cm line which was the inner radius of the multi ring electrodes.

circle, measured one hit position. The hodoscope measured the signals for 4 scintillator bars as shown by the red color boxes. We could draw the dashed line for the track of this cosmic ray event. The detector could capture the cosmic event very well.

5. Summary

We reported the progress of the $\bar{H}$ beam production experiment for the microwave spectroscopy of $\bar{H}$ hyperfine splitting. The double cusp trap was developed to improve the beam intensity of the $\bar{H}$

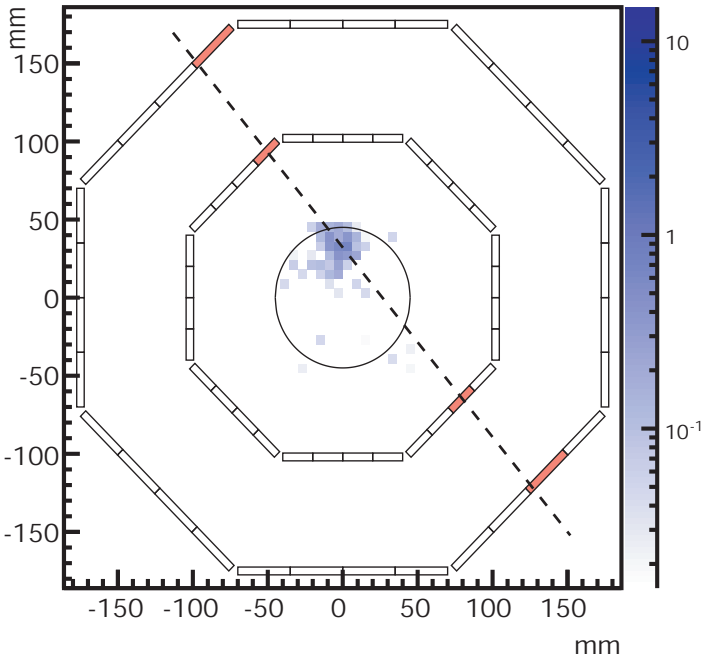

Fig. 10. The example of the cosmic events measured by the $\bar{H}$ beam detector.

atomic beams. We succeeded in producing $\bar{H}$ atoms in the double cusp trap. The AMT was developed and demonstrated to monitor the mixing of antiprotons and positrons. The $\bar{H}$ beam detector was developed. We are in progress toward the measurement of the hyperfine splitting of $\bar{H}$ atoms.

Acknowledgements

This work was supported by the Grant-in-Aid for Specially Promoted Research (19002004 and 24000008) of Japanese Ministry of Education, Culture, Sports, Science and Technology (MEXT), Special Research Projects for Basic Science of RIKEN, RIKEN FPR program, RIKEN IRU program, European Research Council under European Union's Seventh Framework Programme (FP7/2007.2013) / ERC Grant agreement (291242), the Austrian Ministry for Science and Research, Università di Brescia, and Instituto Nazionale di Fisica Nucleare.

References

[1] Y Yamazaki and S Ulmer: Ann. Physik **525** (2013) 493.
[2] G. B. Andresen et al.: Nature **468** (2010) 673.
[3] G. Gabrielse et al.: Phys. Rev. Lett. **108** (2012) 113002.
[4] B. Juhász and E. Widmann : Hyperfine Interact **193** (2009) 305.
[5] N. Kuroda et al: Nat. Commun. **5** (2014) 3089.
[6] A. Kostelecky and N. Russell: Rev. Mod. Phys. **83** (2011), 11.
[7] R. Bluhm et al.: Phys. Rev. Lett. **82** (1999) 2254.
[8] D. Rovera et al.:Phys. Rev. Lett. **107** (2011) 203001.
[9] N. Ramsey, Atomic hydrogen hyperfine structure experiments. Quantum Electrodynamic ed. T. Kinoshita World Scientific (1990) 673.
[10] K.A. Olive et al. (Particle Data Group): Chin. Phys. C, **38**, (2014) 090001.
[11] A Mohri and Y Yamazaki: Europhys. Lett. **63** (2003) 207.
[12] Y. Enomoto *et al* 2010 *Phys. Rev. Lett.* **105** 243401.
[13] Y Nagata and Y Yamazaki: New. J. Phys. **16** (2014) 083026.

[14] Y. Nagata et al.: Journal of Physics Conference Series **635** (2015) 022062.
[15] N. Kuroda et al.: Phys. Rev. Lett. 94, 023401 (2005)
[16] N. Kuroda et al.: Phys. Rev. Lett. 100, 203402 (2008)
[17] N. Kuroda et al.: Phys. Rev. ST Accel. Beams **15** (2012) 0247021.
[18] H. Imao et al.: Hyperfine Interact. **194** (2009) 71.
[19] M. Shibata et al.: Rev. Sci. Instrum. 79, 015112 (2008)
[20] B. Radics et al.: Rev. Sci. Instrum., **86** (2015) 083304.
[21] B. Radics et al.: Measurements and 3D reconstruction of antimatter annihilations with ASACUSA Micromegas tracker. In this proceedings.
[22] N. Kuroda et al.: Antihydrogen synthesis in a double cusp trap. In this proceedings.
[23] M. Tajima et al.: Manipulation and transport of antiprotons for an efficient production of antihydrogen atoms. In this proceedings.
[24] R. Lundmark et al.: J. Phys. B: At. Mol. Opt. Phys **48** (2015) 184001
[25] M. Diermaier et al.: Hyperfine Interactions **233** (2015) 1.
[26] Y. Nagata et al.: The developement of the antihydrogen beam detector: toward the three dimensional tracking with a BGO crystal and a hodoscope. In this proceedings.